

Synthesis, characterization, and polarized luminescence properties of platinum(II) complexes having a rod-like ligand†

Takeshi Sato,* Hiroshi Awano, Osamu Haba, Hiroshi Katagiri, Yong-Jin Pu, Tatsuhiro Takahashi and Koichiro Yonetake

Received 11th January 2012, Accepted 2nd May 2012

DOI: 10.1039/c2dt30071k

We have synthesized a series of platinum (Pt) complexes having a rod-like ligand: 'Pt(F₂PPy)acac', 'Pt(12F₂PPy)acac', and 'Pt(12F₂PPyO₄)acac'. The crystal form of Pt(12F₂PPy)acac was successfully determined to be triclinic by single-crystal X-ray structural analysis. The molecules were parallelly aligned in the unit cell. Monomer and excimer emissions of Pt(12F₂PPy)acac were observed in hexane solution, poly(methyl methacrylate) film, and various nematic LCs. Homogeneous LC cells with the Pt complex/LC mixtures exhibited polarized optical emission resulting from monomer and excimer states. The PL intensity perpendicular to the orientation direction was higher than the parallel one in the whole wavelength region of the Pt complex and the polarization ratio of the excimer was higher than that of the monomer. The polarization ratios of the excimers were estimated to be 1.4–2.5 in nematic LC at room temperature, and decreased gradually with increasing temperature. The polarization ratios of Pt(12F₂PPyO₄)acac were higher than those of Pt(F₂PPy)acac and Pt(12F₂PPy)acac in all the LCs.

Introduction

Organometallic complexes, such as iridium, platinum (Pt), and osmium complexes, have attracted great interest from the points of both basic and applied research. For example, chemical sensors and photocatalysts are well-known applications.^{1–4} Furthermore, high internal quantum efficiency of the organometallic complexes is much effective in organic light emitting diodes (OLEDs), as the strong spin-orbital coupling allows efficient phosphorescence at room temperature (RT).^{5–7} The emission wavelength and luminescent efficiency depend on its ligands, because the ligand molecular orbitals have an influence on the metallic atom d-orbitals.^{8–10} Thus, it is important to examine the crystal structures and photophysical properties of the organometallic complexes. Particularly, square planar Pt(II) complexes are well-known examples of revealing unique luminescence affected by the structure or dispersion state, e.g., excimer or metal–metal-to-ligand charge transfer (MMLCT) emission.^{11–13}

Whereas many studies of highly efficient emitting materials have been carried out to improve the performance of OLED devices, the polarized optical emission properties of organic materials have been also investigated.^{14–17} The polarized optical emitting devices can reduce the light loss of a liquid crystal display (LCD) backlight, by cutting out a polarizing plate, and

they probably improve the light extraction efficiency of an OLED device due to an effect of their horizontal molecular orientation.¹⁸ Moreover, if control of polarizing axis in each pixel is possible, it will be applicable to 3D displays.^{19,20}

The linearly polarized emitting device requires uniaxial molecular orientation. This can be performed using liquid crystalline materials. For example, an oriented liquid crystalline polyfluorene derivative, a well-known blue-emitting conjugated polymer, generated high polarized optical emission.²¹ In a luminescent material and liquid crystal mixture, the temperature dependence of the polarized emitting properties has been investigated.²² The order parameter evaluated by polarized absorption spectroscopy decreased steeply when the temperature approached the smectic/isotropic phase transition temperatures.

The above devices used fluorescent materials. On the other hand, polarized emission of lanthanide(III) complexes has been obtained with the aid of the stretched polymer film technique,²³ and lanthanide(III) complexes doped into a nematic LC also showed polarized luminescence.^{24,25} Moreover, circularly polarized light was measured in single crystals of lanthanide(III) complexes.²⁶ Recently, a discotic-like Pt complex exhibited polarized phosphorescent emission perpendicular to the axis of the columnar stack,²⁷ and metallomesogens based on Pt complexes exhibiting smectic LC generated comparatively high polarized emission using rubbed polymer layers.^{28,29} However, few studies into the relationship between molecular orientation and polarized emission of the organometallic complexes have been carried out.

In this study, we have synthesized a series of platinum (Pt) complexes: platinum(II) (2-(5',6'-difluorophenyl)pyridinato-*N*, *C*2') (2,4-pentanedionato-*O*,*O*) (Pt(F₂PPy)acac), platinum(II) (2-(4'-dodecyl-5',6'-difluorophenyl)pyridinato-*N*,*C*2') (2,4-

Graduate School of Science and Engineering, Yamagata University, 4-3-16 Jonan, Yonezawa, Yamagata 992-8510, Japan.
E-mail: twn34755@st.yamagata-u.ac.jp; Tel: +81-238-26-3047

† Electronic supplementary information (ESI) available. CCDC 854595. For ESI and crystallographic data in CIF or other electronic format see DOI: 10.1039/c2dt30071k

pentanedionato-*O,O*) (Pt(12F₂PPy)acac), platinum(II) (2-(4'-dodecyl-5',6'-difluorophenyl)-5-butoxypyridinato-*N,C2'*) (2,4-pentanedionato-*O,O*) (Pt(12F₂PPyO4)acac), which have a β-diketonato ligand (O[^]O) and monoanionic cyclometalating ligand (C[^]N). We have analyzed the crystal structure, thermal behavior, and photophysical properties of Pt(12F₂PPy)acac mainly. Furthermore, we have investigated the unique polarized optical emission properties of the three Pt complexes in several nematic LCs, and discussed the effect of the molecular structure of the ligand on the polarization ratio.

Results and discussion

Synthesis and thermal decomposition temperature of Pt complexes

Pt(F₂PPy)acac, Pt(12F₂PPy)acac, and Pt(12F₂PPyO4)acac were prepared through 2, 4, and 5 steps, respectively, as shown in Scheme 1. The starting material for synthesis of Pt(12F₂PPy)acac and Pt(12F₂PPyO4)acac is 1,2-difluorobenzene (**1**), and that for Pt(F₂PPy)acac is 2,3-difluorophenyl boronic acid (**3**). All aryl–aryl coupling reactions were conducted by Suzuki–Miyaura cross coupling reactions using aryl halide and boronic acid compounds. A key reaction step is direct alkylation to **1** which is *ortho*-lithiated by 2.6 M solution of butyllithium (*n*-BuLi). The reaction proceeded under warming to RT after adding 1-iodododecane to the activated **1** in THF solution at –40 °C. The unreacted 1-iodododecane in the residue was changed to alcohol or alkene derivatives by reaction with base. The resulting mixture was purified by column chromatography to give pure alkylated compound **2**. The target Pt complexes were prepared by a complexation of the aryl–pyridyl ligands (**5**, **6**, and **9**) with K₂PtCl₄ followed by a reaction with acetylacetonate. The Pt complexes were fully characterized by ¹H-NMR, FT-IR spectral data, and elemental analyses. The thermal decomposition temperatures

of Pt(F₂PPy)acac, Pt(12F₂PPy)acac, and Pt(12F₂PPyO4)acac were estimated to be 267, 289, and 289 °C, respectively, by thermogravimetric analysis (TGA).

Crystal structure and phase transition properties of Pt(12F₂PPy)acac

A single crystal of Pt(12F₂PPy)acac was grown from a dilute hexane solution in a refrigerator and characterized using X-ray crystallography. Fig. 1 shows the molecular structure of Pt(12F₂PPy)acac in the single crystal. The ORTEP drawing is shown in the supporting information (Fig. S1†). Pt(12F₂PPy)acac has a planar geometry including a long alkyl chain moiety which extends inside the molecule, as the dihedral angle between the plane of the aromatic ring and carbon chain (C11–C10–C12–C13) is 3.4(5)°. The platinum atom is located just in the mean plane of both the aryl–pyridine and the β-diketonato ligand (0.0255(9) Å). There is very little distortion away from the square plane. The O–Pt–O and C–Pt–N bond angles are 91.82(10) and 81.91(14)°. The Pt–C6, Pt–O1, Pt–O2, and Pt–N bond lengths are 1.960(4), 2.004(3), 2.084(3), and 1.991(3) Å, respectively. They are typical bond angles and lengths for cyclometalates and β-diketonate derivatives of Pt.^{30,31}

The pertinent details of X-ray crystallography are given in Table 1. The crystal packing of Pt(12F₂PPy)acac is shown in Fig. 2. This complex crystallizes in the triclinic *P* $\bar{1}$ space group.

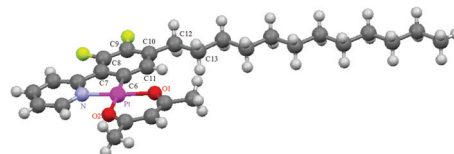
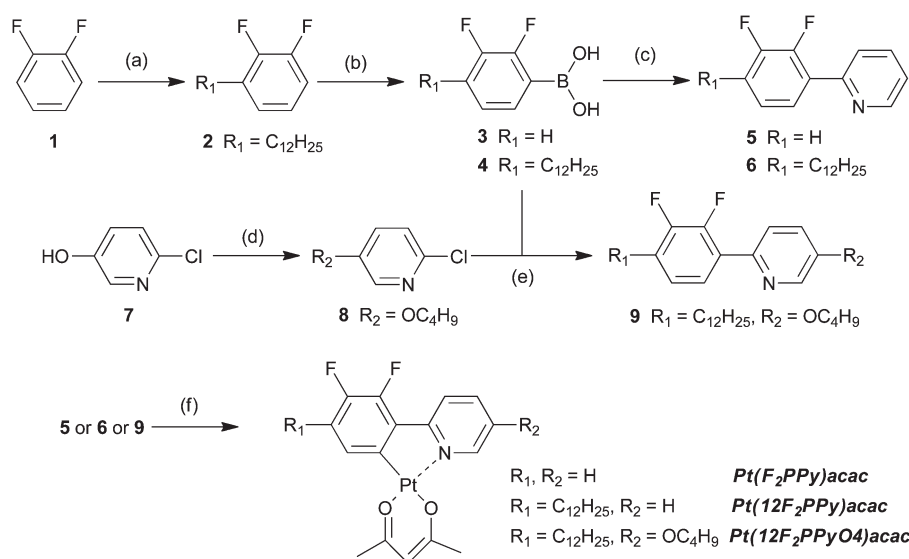


Fig. 1 The molecular structure of Pt(12F₂PPy)acac.

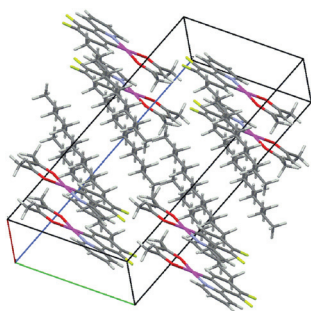


Scheme 1 Synthesis of Pt(F₂PPy)acac, Pt(12F₂PPy)acac, and Pt(12F₂PPyO4)acac. Conditions: (a) 1) *n*-BuLi, hexane, THF, –78 °C, 2) 1-iodohexane –40 °C; (b) 1) *n*-BuLi, hexane, THF, –78 °C, 2) B(OMe)₃, THF, –78 °C, 3) HCl, RT; (c) 2-bromopyridine, Pd(PPh₃)₄, 2M K₂CO₃aq., THF, 70 °C, (d) 1-iodobutane, K₂CO₃, 2-butanone, 60 °C, (e) 1) K₂PtCl₄, 2-ethoxyethanol, water, 80 °C, 2) acetylacetonate, Na₂CO₃, 2-ethoxyethanol, 100 °C.

Table 1 Crystal data for Pt(12F₂PPy)acac

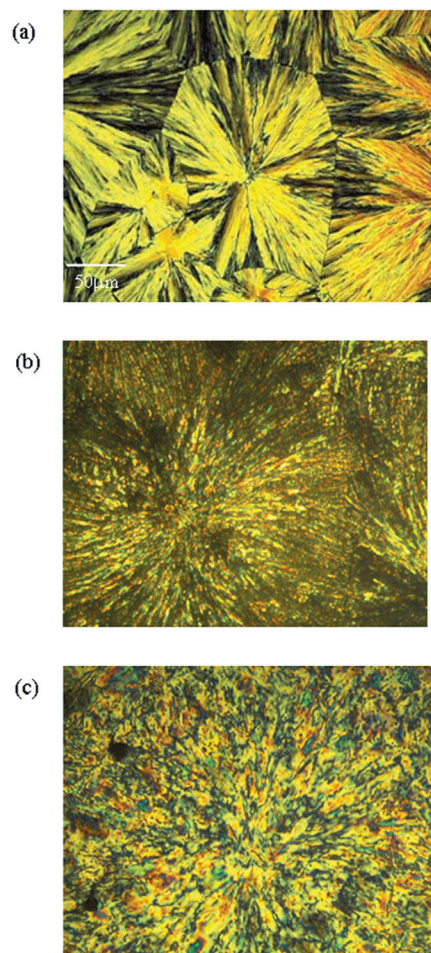
Compound	Pt(12F ₂ PPy)acac
Chemical formula	C ₂₈ H ₃₇ F ₂ NO ₂ Pt
Color	Yellow
Formula Weight	652.68
Crystal system	Triclinic
<i>a</i> /Å	5.4867(13)
<i>b</i> /Å	11.059(3)
<i>c</i> /Å	21.565(5)
α /°	81.946(7)
β /°	84.414(8)
γ /°	82.446(7)
Unit cell volume/Å ³	1280.2(5)
Temperature/K	103
Space group	<i>P</i> $\bar{1}$
No. of formula units per unit cell, <i>Z</i>	2
No. of reflections measured	19 375
No. of independent reflections	5834
<i>R</i> _{int}	0.0484
Final <i>R</i> ₁ values (<i>I</i> > 2σ(<i>I</i>))	0.0315
Final <i>wR</i> (<i>F</i> ²) values (<i>I</i> > 2σ(<i>I</i>))	0.0621
Final <i>R</i> ₁ values (all data) ^a	0.0378
Final <i>wR</i> (<i>F</i> ²) values (all data) ^b	0.0653

$$^a R_1 = \sum ||F_o| - |F_c|| / \sum |F_o|. \quad ^b wR(F^2) = \{ \sum [w(F_o^2 - F_c^2)^2] / \sum [w(F_o^2)^2] \}^{1/2}.$$

**Fig. 2** The crystal packing of Pt(12F₂PPy)acac.

In the unit cell, the closest aligned two Pt complexes are slightly off in a parallel direction, and they are stacked along their long alkyl chains. Also, the alkyl chains are face to face and interdigitate with each other (Fig. 2). The average separation between the aryl ring (C6–C11) and mean plane of the pyridine ring is 3.363(5) Å. On the other hand, this situation can be regarded as each alkyl chain facing to the anti-parallel direction (see Fig. S2 in ESI†). In this case, the distance between two mean planes of the pyridine moieties is 3.326(5) Å. The dimers in both parallel and anti-parallel directions have a plane-to-plane separation of 3.3–3.4 Å, indicative of moderate π – π interaction. However, there is no Pt–Pt bond because the Pt–Pt distances in the parallel and anti-parallel directions are 5.487(1) and 6.703(1) Å, respectively.

Fig. 3 shows optical textures of Pt(12F₂PPy)acac observed under a polarizing optical microscope (POM) with crossed polarizers. Cooling Pt(12F₂PPy)acac from the isotropic phase, a spherulitic texture started growing at 55 °C. The spherulites shown in Fig. 3(a) were observed and stored at ambient temperature. After 5 days, the optical structure was changed by maintaining at ambient temperature, as shown in Fig. 3(b). After subsequent heating to 90 °C, the optical texture was changed (Fig. 3(c)). These structural changes indicating solid–solid phase

**Fig. 3** POM images of Pt(12F₂PPy)acac (a) cooled from the melt, (b) after 5 days and (c) at 90 °C on subsequent heating.

transitions were confirmed by DSC measurement and X-ray diffraction analysis (see Fig. S3 and S4 in ESI†). Pt(12F₂PPy)acac single crystal exhibited two phase transitions. On the other hand, the sample cooled from the melt showed only the isotropic phase transition. The XRD pattern of the sample was not identical to that of the single crystal (Fig. S4†), and the d-spacing values of the reflections were not consistent with those of the single crystal. The crystal forms after heating were definitely different from that of the single crystal. Thus, Pt(12F₂PPy)acac exhibits metastable states, and the crystallization is very slow.

Photophysical properties of Pt(12F₂PPy)acac

Fig. 4 shows ultra violet–visible light (UV–vis) absorption spectra of Pt(12F₂PPy)acac in hexane and chloroform solutions. They show two absorption maxima in the wavelength of 200–300 nm whose molar extinction coefficients (ϵ) were higher than 10 000 M^{−1} cm^{−1}, suggesting high energy transition. The high energy absorption bands can be assigned to a ¹ π – π^* ligand centered (¹LC) transition because the spectrum of Pt(12F₂PPy)acac in this range was analogous to that of the ligand (12F₂PPy), whose peaks were observed at 246 and 278 nm in chloroform solution.

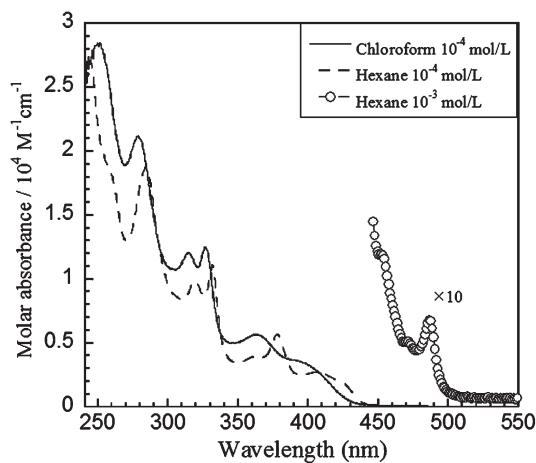


Fig. 4 UV-vis absorption spectra of Pt(12F₂PPy)acac in chloroform and hexane solutions.

The molar absorbance of the bands from 350 to 440 nm, on the other hand, was lower than $6000 \text{ M}^{-1} \text{ cm}^{-1}$, and the spectrum profile of the hexane solution was evidently different from that of the chloroform solution in this range. Characteristics of low ϵ value and solvatochromism are observed in MLCT transition.¹¹ Thus, they are assigned to $d-\pi^*$ metal-to-ligand charge transfer (¹MLCT) transitions. In addition, a weak band at 487 nm was observed in the spectrum of $10^{-3} \text{ mol L}^{-1}$ hexane solution. The low extinction of this band ($\epsilon = 68 \text{ M}^{-1} \text{ cm}^{-1}$) suggests a transition to the triplet excited state enabled by spin-orbit coupling (³MLCT).³²

Fig. 5 shows PL and excitation spectra of Pt(12F₂PPy)acac in hexane solution. The PL spectra of the solutions with three different concentrations (10^{-3} , 10^{-4} , and $10^{-5} \text{ mol L}^{-1}$) are approximately consistent, and their intensity maxima are at around 490 and 520 nm. This indicates monomer emission of Pt(12F₂PPy)acac due to MLCT or mixed ³LC-MLCT states. The spectrum of the high concentration solution ($10^{-3} \text{ mol L}^{-1}$) exhibited a broad emission band at longer wavelength region ($\lambda_{\text{max}} = 648 \text{ nm}$). It possibly results from excimer state or MMLCT transition due to a weak Pt-Pt bond. The excitation spectrum of $10^{-3} \text{ mol L}^{-1}$ hexane solution for 490 and 650 nm was analogous. The result revealed that the two emissions were originated from the same ground state species, *i.e.*, the broad emission at around 650 nm is generated from the excimer.³⁰ No broad emission was observed in the chloroform solution, because the polar Pt complex can be well dissolved in the polar chloroform compared to non-polar hexane.

Pt(12F₂PPy)acac neat film and Pt(12F₂PPy)acac/poly(methyl methacrylate) (PMMA) films were prepared by spin coating to explore further emission properties. The photoluminescence quantum yield (PLQY) of 2 wt% Pt(12F₂PPy)acac/PMMA film was 0.52, and the lifetime was 9.0 μs at 5 K, which is comparable with that of other platinum complexes.^{11,12,32}

PL spectra of all the films exhibited the monomer emission at around 490 nm, as shown in Fig. 6. The excimer emission appeared clearly in the neat film and 20 wt% Pt(12F₂PPy)acac/PMMA film. In brief, Pt(12F₂PPy)acac easily came to form the excimer with increasing the concentration. The PL intensity maxima of the excimer emission for the Pt(12F₂PPy)acac/

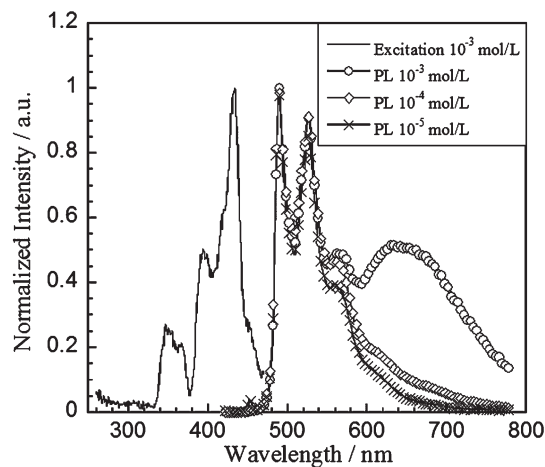


Fig. 5 PL and excitation spectra of Pt(12F₂PPy)acac in hexane solution.

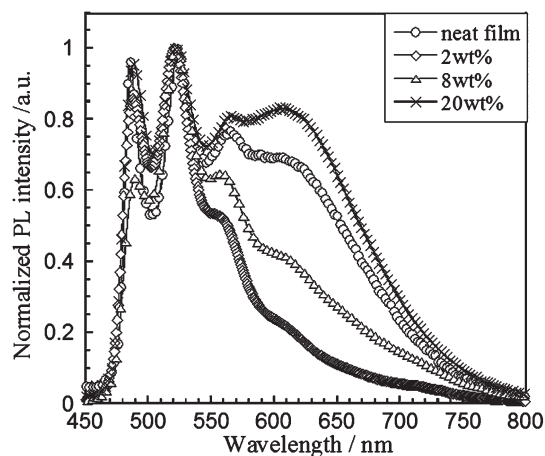


Fig. 6 PL spectra of Pt(12F₂PPy)acac neat film and doped PMMA films.

PMMA film and the neat film were observed at 619 and 626 nm, respectively. They were blue shifted by 20–30 nm compared with the solution due to the difference in their polarities between the polymer matrix and solvent.

Polarized optical emission properties of Pt complexes

Pt(F₂PPy)acac (1.9 wt%), Pt(12F₂PPy)acac (2.6 wt%), and Pt(12F₂PPyO₄)acac (2.9 wt%) were completely dissolved into various nematic LCs. All the mixtures exhibited a nematic phase at ambient temperature and no crystallization of the Pt complexes in LCs was confirmed by POM observation and DSC measurement. The PL spectra revealed two sharp emission peaks at 490–510 and 520–550 nm, and broad emission at around 630–680 nm at ambient temperature, which were analogous to those of the high concentration solution and film shown in Figs 5 and 6, respectively. Thus, the excimer emission was also observed in the Pt complex/LC mixtures.

The Pt complex/LC mixtures were injected into LC cells as described in the Experimental section. In the LC cells,

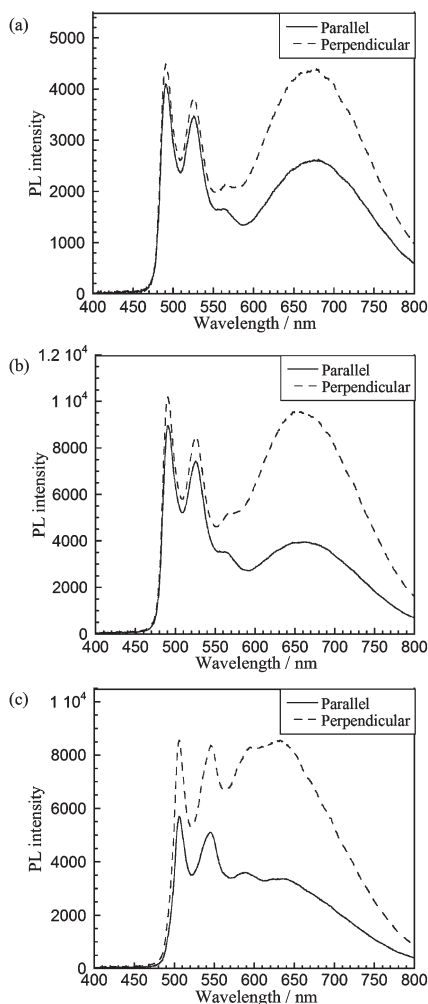


Fig. 7 Linearly polarized PL spectra of (a) Pt(F₂PPy)acac, (b) Pt(12F₂PPy)acac, and (c) Pt(12F₂PPyO₄)acac in MLC-6608 at 20 °C. The solid line and dotted line are for the polarizer aligned parallel and perpendicular to the rubbing direction, respectively.

homogeneous alignment parallel to the rubbing direction was observed under the POM with crossed polarizers. Fig. 7 shows polarized PL spectra of the Pt complexes/MLC-6608 cells which were measured through a polarizer, when the direction of the molecular alignment in the cells was in parallel and perpendicular positions with the transmission axis of the polarizer. In the cells, the PL intensities in the perpendicular position were higher than those in the parallel position in the whole emission wavelength region of Pt complexes. Similar luminescence behaviors were obtained in the other cells. Thus, they evidently showed polarized optical emission.

It is noteworthy that the polarized optical emission of the Pt complexes was generated in the direction perpendicular to the molecular-orientation direction. The polarized monomer and excimer emissions are assigned to MLCT or mixed ³LC-MLCT emission. It suggests that the polarized optical emission results from intramolecular and intermolecular electronic transitions along the ligand to Pt direction, *i.e.*, the transition dipole moment is approximately perpendicular to the molecular axis of the ligand. The polarization ratio (*P*) and order parameter (*S*) were estimated to explore the polarized optical emission by the following equations;

$$P = \frac{PL_{\text{perp}}}{PL_{\text{para}}}$$

$$S = \frac{PL_{\text{perp}} - PL_{\text{para}}}{PL_{\text{perp}} + 2PL_{\text{para}}}$$

where PL_{para} and PL_{perp} denote maximum intensities of the parallel and perpendicular spectra, respectively. The *P* and *S* values of the cells measured at 20 °C were summarized in Table 2.

The *P* and *S* values of the three Pt complexes in the same LC host compound were notably different; Pt(F₂PPy)acac < Pt(12F₂PPy)acac < Pt(12F₂PPyO₄)acac. The result indicates that the orientation ability of a Pt complex in a nematic LC has a significant effect on the polarized luminescence properties. That is,

Table 2 Nematic/isotropic phase transition temperatures (T_{NI}), polarization ratios (*P*), and order parameters (*S*) of the Pt complex/LC mixtures. The *P* and *S* values were taken at 20 °C

Sample Nematic LC mixtures	T_{NI} (°C)	<i>P</i>		<i>S</i>	
		Monomer	Excimer	Monomer	Excimer
Pt(F ₂ PPy)acac/5CB	N 35.4	1.18	1.45	0.058	0.13
Pt(12F ₂ PPy)acac/5CB	N 35.2	1.08	1.66	0.027	0.18
Pt(12F ₂ PPyO ₄)acac/5CB	N 35.2	1.5	1.97	0.14	0.24
Pt(F ₂ PPy)acac/E7	N 58.8	0.97	1.7	-0.011	0.19
Pt(12F ₂ PPy)acac/E7	N 58.2	1.17	2.09	0.054	0.27
Pt(12F ₂ PPyO ₄)acac/E7	N 58.3	1.6	2.31	0.17	0.3
Pt(F ₂ PPy)acac/JD-7000XX	N 69.8	1.13	1.71	0.041	0.19
Pt(12F ₂ PPy)acac/JD-7000XX	N 70.2	1.15	2.22	0.047	0.29
Pt(12F ₂ PPyO ₄)acac/JD-7000XX	N 69.4	1.5	2.53	0.14	0.34
Pt(F ₂ PPy)acac/JD-5023XX	N 75.4	1.24	1.72	0.074	0.19
Pt(12F ₂ PPy)acac/JD-5023XX	N 75.0	1.21	2.23	0.066	0.29
Pt(12F ₂ PPyO ₄)acac/JD-5023XX	N 75.5	1.59	2.32	0.17	0.31
Pt(F ₂ PPy)acac/ZLI-4792	N 89.1	1.24	1.72	0.074	0.19
Pt(12F ₂ PPy)acac/ZLI-4792	N 91.7	1.23	2.35	0.07	0.31
Pt(12F ₂ PPyO ₄)acac/ZLI-4792	N 89.7	1.63	2.53	0.17	0.34
Pt(F ₂ PPy)acac/MLC-6608	N 90.3	1.09	1.69	0.031	0.19
Pt(12F ₂ PPy)acac/MLC-6608	N 91.8	1.14	2.44	0.044	0.32
Pt(12F ₂ PPyO ₄)acac/MLC-6608	N 92.7	1.5	2.54	0.14	0.34

long alkyl and alkoxy chains facilitate the molecular orientation for the Pt complex along the long axis of LC molecules. Pt(12F₂PPyO₄)acac/MLC-6608 cell showed the highest *P* and *S* values in this study, which were estimated to be 2.54 and 0.34 in the excimer.

The *P* and *S* values of the excimer are distinctly higher than those of the monomer. The thermal agitation of the excimer is possibly lower in the LC state because of the bulky and rod-like shape of the excimeric Pt complex. The transition moment in the monomeric Pt complex, on the other hand, probably has a directional bias between Pt atom and aryl-pyridyl ligand. It is hard to explain the polarized optical emission in detail in terms of above limited data, and further experimental evidence and theoretical examination are needed to ensure our conjecture.

The PL spectrum of a Pt complex is affected by temperature change.^{13,33} We have investigated the temperature dependence of

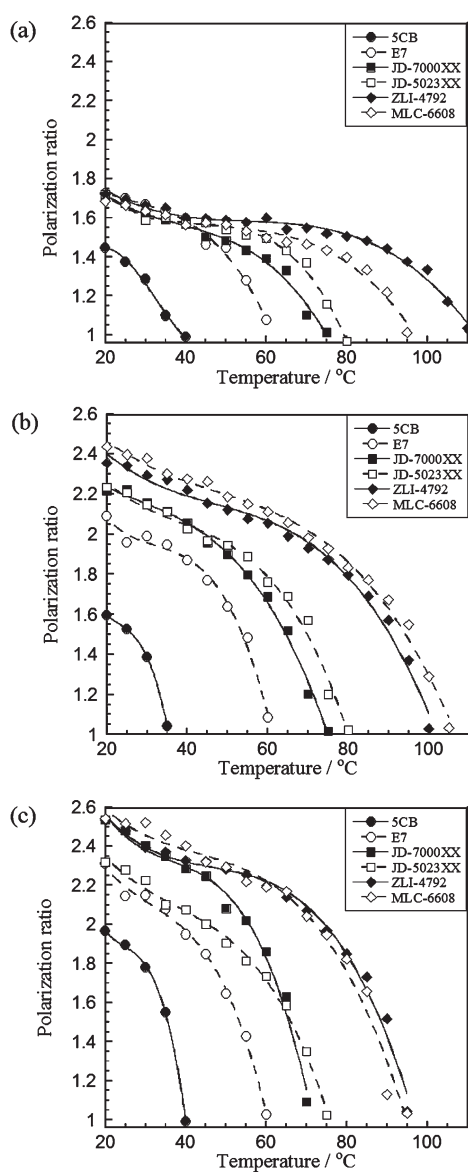


Fig. 8 The temperature dependence of polarization ratios of the excimers in (a) Pt(F₂PPy)acac/LC, (b) Pt(12F₂PPy)acac/LC, and (c) Pt(12F₂PPyO₄)acac/LC cells.

the polarized luminescent properties by focusing attention on the excimer emission. The *P* values of all the samples gradually decreased with increasing temperature, and ended up at 1.0 at the isotropic phase, as shown in Fig. 8. Much the same is true for the monomers (see Fig. S5 in ESI†). Thus, the polarized luminescence depends on the order parameter of the nematic LC and molecular orientation of each Pt complex.

In the Pt(F₂PPy)acac/LC cells, the same *P* values were obtained in the lower temperature range except for the case of 5CB. In the Pt(12F₂PPy)acac/LC and Pt(12F₂PPyO₄)acac/LC cells, on the other hand, the *P* values were not the same even in the low temperature range. The values of Pt complex/5CB cells were comparatively lower than the other LC mixtures in the temperature range. In general, the order parameter of the LC decreases drastically at around the nematic/isotropic phase transition temperature (*T*_{N/I}). Hence, the low *P* and *S* values in the case of 5CB are probably due to the comparatively large thermal agitation caused by the low *T*_{N/I} close to ambient temperature. These results suggest that the polarized optical emission depends on the matrix LC and molecular structures of the ligand.

Fig. 9 presents changes in the maximum PL emission wavelengths (PL- λ_{max}) of the excimer emission in Pt(12F₂PPy)acac/LC cells. They increased with elevating temperature, suggesting a red-shift. For example, the PL- λ_{max} of the excimer emission for Pt(12F₂PPy)acac/MLC-6608 red-shifted from 650 nm at 20 °C to 694 nm at 105 °C. The other Pt complex/LC cells showed the same tendency. Increasing the molecular movement allowed closer excimer formation and rearrangement in the nematic LC, giving stronger π - π interactions.

Fig. 10 shows the PL spectra in the perpendicular direction for Pt(12F₂PPy)acac/MLC-6608 cell. The PL intensities in the entire wavelength region decreased with increasing temperature as the PL intensities of the monomer became relatively low compared to those of the excimer. The same behavior was also observed in the parallel direction. The intensity ratio of the monomer/excimer at PL- λ_{max} were plotted against temperature in Fig. 11. They decreased with increasing temperature. This is due to a diffusion-controlled process and a difference in the thermal stability between the monomer and the excimer.³⁴ In the

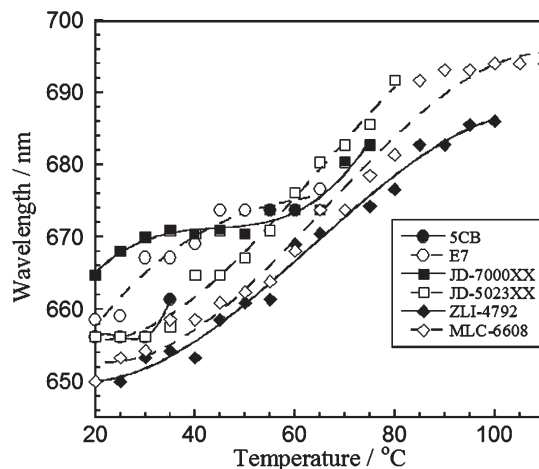


Fig. 9 The temperature dependence of maximum wavelengths of the excimers in Pt(12F₂PPy)acac/LC cells.

nematic LC state, the molecular mobility of the Pt complex is comparatively high, and it probably enhances the encounter of the Pt complexes to form the excimer. On the other hand, Pt(12F₂PPyO₄)acac/LC cells show an intriguing behavior. The intensity ratios in the parallel position decreased definitely around T_{NI} (Fig. 11(e)). This was maybe caused by decreased viscosity and thermal agitation. The ratio in the perpendicular one showed convex curves suggesting the existence of a

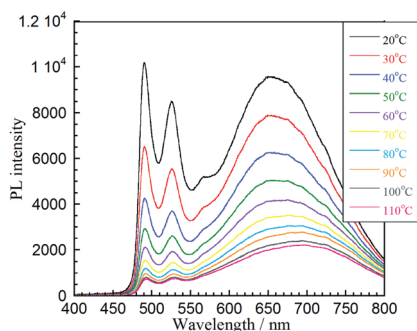


Fig. 10 Temperature-dependent emission spectra of Pt(12F₂PPy)acac (2.6 wt%)/MLC-6608 cell in the perpendicular direction.

dissociation-controlled process (Fig. 11(f)). This behavior was possibly determined by the correlation between diffusion- and dissociation-controlled processes.

We have examined the temperature dependence of the PL intensities for the Pt complexes doped PMMA film to clarify the influence of the molecular movement of Pt(12F₂PPy)acac on the excimer formation. Fig. 12 shows the PL intensities of the monomer and excimer for 20 wt% Pt(12F₂PPy)acac doped PMMA film comparably decreased with increasing temperature. The PL intensity ratio of the monomer/excimer remained almost unchanged under 80 °C close to the melting temperature of Pt(12F₂PPy)acac and the glass transition of PMMA, as shown in Fig. S6.† This suggests the molecular movement of Pt(12F₂PPy)acac was inhibited in the PMMA film by its high viscosity. The decreasing PL intensity was chiefly caused by the temperature dependence of their PLQY.³³ Therefore, the excimer formation and subsequent emission are influenced by the mobility and diffusion of the Pt complexes in the nematic LC state.

Conclusions

We have synthesized a series of Pt complexes; 'Pt(F₂PPy)acac', 'Pt(12F₂PPy)acac', and 'Pt(12F₂PPyO₄)acac' having a rod-like

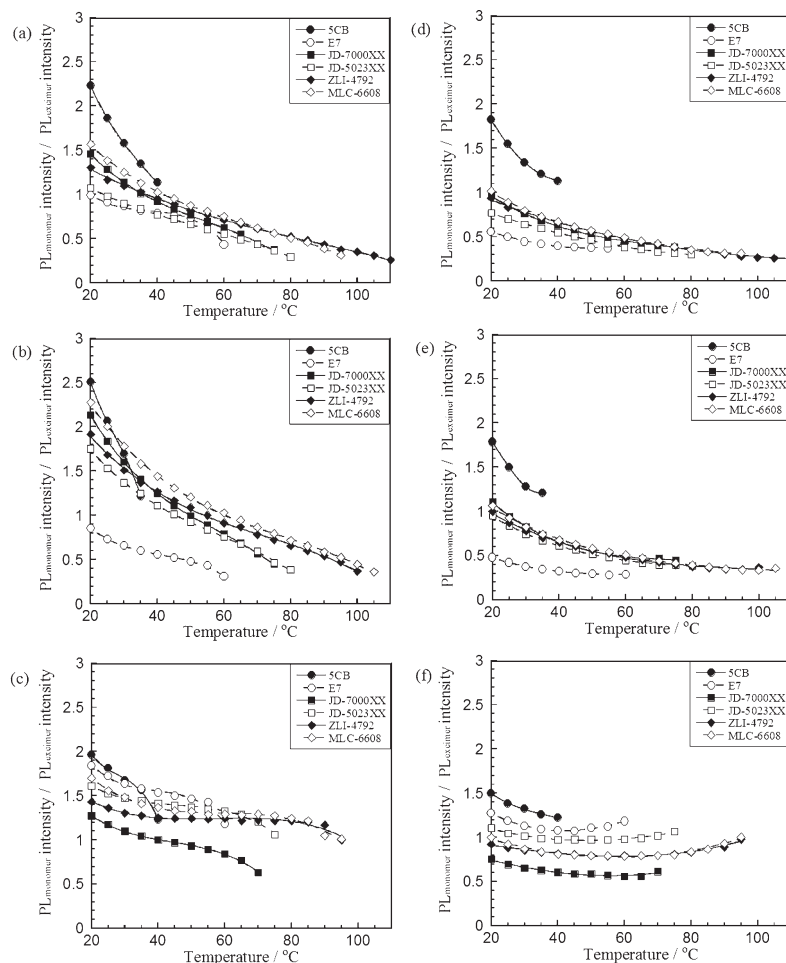


Fig. 11 Changes in PL intensity ratios of the monomer/the excimer of (a) Pt(F₂PPy)acac/LC, (b) Pt(12F₂PPy)acac/LC, and (c) Pt(12F₂PPyO₄)acac/LC cells in the parallel direction, (d) Pt(F₂PPy)acac/LC, (e) Pt(12F₂PPy)acac/LC, and (f) Pt(12F₂PPyO₄)acac/LC cells in the perpendicular direction.

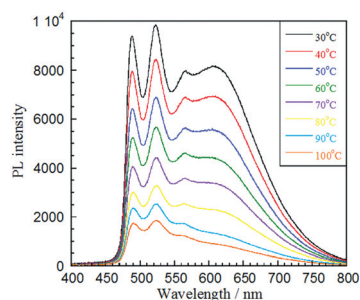


Fig. 12 Temperature-dependent emission spectra of Pt(12F₂PPy)acac (20 wt%)/PMMA thin film.

ligand. The crystal form of Pt(12F₂PPy)acac was successfully determined to be triclinic: $a = 5.4867(13)$ Å, $b = 11.059(3)$ Å, $c = 21.565(5)$ Å, $\alpha = 81.946(7)^\circ$, $\beta = 84.414(8)^\circ$, $\gamma = 82.446(7)^\circ$ by single-crystal X-ray structural analysis. In the unit cell, the closest two Pt complexes are stacked slightly off in a parallel direction, and other Pt complex interdigitates on the part of the long alkyl group. However, there is no Pt–Pt bond in the dimer states. The DSC, POM, and X-ray diffraction analysis revealed the presence of a metastable structure. The UV–vis absorption spectra showed an intense transition (¹LC) state, and solvatochromic band (¹MLCT). Moreover, a weak absorption peak at 487 nm was also observed in high concentration hexane solution, implying a ³MLCT band. The hexane solution displayed monomer and excimer emission at around 490 and 650 nm, respectively. The Pt complexes dissolved in nematic LCs showed homogeneous alignment between two glass substrates with rubbed polyimide. The uniaxially-oriented samples exhibited a linearly polarized luminescence perpendicular to the orientation direction. Particularly, the excimer emission showed comparatively high polarization ratio. The highest polarization ratio amounted to 2.54 in the Pt(12F₂PPyO₄)acac/MLC-6608 cell at RT. The polarization ratios of Pt(12F₂PPyO₄)acac were higher than those of Pt(F₂PPy)acac and Pt(12F₂PPy)acac in all the LCs. The polarization ratios of all the samples gradually decreased with increasing temperature, finally coming to 1.0 in the isotropic phase. Additionally, the emission wavelengths were red-shifted about 40 nm at most with increasing temperature. The molecular movement of the Pt complex is important factor to form an excimer in nematic LC. We presently prepare novel smectic LCs to dissolve the Pt complex and investigate the polarization properties in the smectic phase.

Experimental

Measurements

Infrared spectra were recorded on a HORIBA FT-210 spectrometer. NMR spectra were obtained on a JEOL JNM-ECX 400 (400 MHz for ¹H and 100 MHz for ¹³C) spectrometer. Elemental analysis was carried out by a CHNS/O 2400II analyzer (Perkin Elmer). Single crystal X-ray diffraction was carried out by a Saturn 724⁺ (Rigaku Denki) using Mo-K α irradiation. Similar-ADP restraint SIMU was applied to the part of alkyl disorder for the refinement. UV–vis absorption spectra were recorded on a Shimadzu UV3150 spectrometer. Photoluminescence and

excitation spectra were recorded on a HORIBA Jobin Yvon Fluoromax-4 spectrofluorometer. PLQY was measured by a PLQY measurement system C9920-01 (Hamamatsu Photonics). Pt(12F₂PPy)acac was doped into PMMA, and the thin film was cast by spincoating. The PLQY of the film was measured using an integrating sphere under a nitrogen purge. Transient photoluminescence decay was measured by a synchronous delay generator C4792-02 equipped with a streak scope C4334 (Hamamatsu Photonics) under excitation by irradiating a nitrogen laser ($\lambda = 337$ nm, 50 Hz, 800 ps pulses). The thermal decomposition temperature was determined on the basis of 5% decrease in weight by a thermogravimetric analyzer Q-50 (TA instruments). Thermal properties were examined using a differential scanning calorimeter Q-200 (TA instruments) at heating–cooling rates of 10 °C min⁻¹ under a nitrogen purge. X-ray diffraction was carried out by a MicroMax007 R-Axis IV⁺⁺ (Rigaku Denki) using Cu-K α irradiation. The optical textures of the Pt complex and the LC samples were examined using a POM BX-50P (Olympus) equipped with a hot stage TH-600RMS (Linkam). Polarized emitting cells were set on the hot stage, and irradiated by a UV-LED irradiator Aicure UJ30/35 (Panasonic). Polarized photoluminescence spectra were measured through a polarizer with a photonic multichannel analyzer PMA-11 (Hamamatsu Photonics). The polarized PL measurements were taken from the isotropic phase to 20 °C at intervals of 5 °C.

Reagents

1,2-Difluorobenzene (Tokyo Kasei), 1-iodododecane (Kanto Chemicals), 2.6 M solution of *n*-BuLi in *n*-hexane (Kanto Chemicals), trimethyl borate (Alfa Aesar), 2,3-difluorophenyl boronic acid (Tokyo Kasei), tetrakis(triphenyl)phosphine palladium (0) (Pd(PPh₃)₄) (Tokyo Kasei), 2-bromopyridine (Tokyo Kasei), 2-chloro-5-hydroxypyridine (Tokyo Kasei), 1-iodobutane (Kanto Chemicals), potassium tetrachloroplatinate(II) (K₂PtCl₄) (Aldrich), acetylacetone (Kanto Chemicals), 6 mol% aqueous hydrochloric acid (Kanto Chemicals), sodium carbonate (Na₂CO₃) (Kanto Chemicals), potassium carbonate (K₂CO₃) (Kanto Chemicals), anhydrous magnesium sulfate (MgSO₄) (Kanto Chemicals), dry THF (Kanto Chemicals), *n*-hexane (Kanto Chemicals), ethanol (Kanto Chemicals), 2-butanone (Kanto Chemicals), 2-ethoxyethanol (Kanto Chemicals), ethylacetate (Kanto Chemicals), chloroform (Kanto Chemicals), and potassium hydroxide (KOH) (Kanto Chemicals) were purchased and used as received. Unless otherwise noted, the remaining chemicals were commercially available and used without further purification.

Synthesis of ligands

1,2-Difluoro-3-dodecylbenzene (2). To a solution of 1,2-difluorobenzene (**1**) (7.32 g, 64.2 mmol) in dry THF (110 ml), a 2.6 M solution of *n*-BuLi in *n*-hexane (24.9 ml, 64.2 mmol) was added slowly at -78 °C under nitrogen atmosphere. The solution was stirred at -78 °C for 2 h. After 1-iodododecane (19.0 g, 64.2 mmol) was added to the solution at -40 °C, the mixture was allowed to warm to RT and stirred overnight. The solvents were removed by a rotary evaporator, and ethanol (100 ml) and

KOH (2.0 g) was added to the residue. The mixture was stirred at 70 °C for 20 h to remove the unreacted 1-iodododecane. The reaction mixture was diluted with water, and extracted with *n*-hexane. The extract was washed with brine, dried over anhydrous MgSO₄ and concentrated under reduced pressure. The residue was purified by column chromatography with *n*-hexane to give a colorless liquid (11.8 g, 41.8 mmol, 65%).

¹H-NMR (400 MHz, CDCl₃): δ (ppm) = 7.00–6.90 (m, 3H, ArH), 2.66 (t, *J* = 7.7 Hz, 2H, Ar-CH₂-), 1.63–1.55 (m, 2H, Ar-CH₂-CH₂-), 1.38–1.18 (m, 18H, -CH₂-), 0.93 (t, *J* = 7.0 Hz, 3H, -CH₃). IR: ν (cm⁻¹) = 2960, 2930, 2860, 2360, 2340, 1600, 1490, 1210, 827, 773, and 719.

2,3-Difluoro-4-dodecylphenylboronic acid (4). To a solution of **2** (11.8 g, 41.8 mmol) in dry THF (90 ml), 2.6 M solution of *n*-BuLi in *n*-hexane (17.8 ml, 46.0 mmol) was added dropwise at -78 °C under nitrogen atmosphere. After the reaction mixture was stirred for 2 h, previously cooled trimethyl borate (9.1 ml, 58.4 mmol) was added slowly. The reaction mixture was allowed to warm to RT and stirred overnight, and then stirred for 1 h with 6 mol% (50 ml) aqueous hydrochloric acid. The resulting mixture was extracted with diethyl ether, and the organic layer was washed with water several times and dried over anhydrous MgSO₄. The solvents were removed under reduced pressure. The resulting solid was recrystallized from *n*-hexane twice to give white needles (12.2 g, 37.2 mmol, 89%).

¹H-NMR (400 MHz, CDCl₃): δ (ppm) = 7.44 (t, *J* = 7.7 Hz, 1H, ArH), 6.99 (t, *J* = 6.6 Hz, 1H, ArH), 5.1 (d, *J* = 5.9 Hz, 2H, B-OH), 2.67 (t, *J* = 7.7 Hz, 2H, Ar-CH₂-), 1.54–1.67 (m, 2H, Ar-CH₂-CH₂-), 1.40–1.18 (m, 18H, -CH₂-), 0.87 (t, *J* = 7.4 Hz, 3H, -CH₃). IR: ν (cm⁻¹) = 3500–3000, 2960, 2930, 2860, 1640, 1500, 1450, 1340, 1130, 951, and 897.

2-(2,3-Difluorophenyl)pyridine (5). A solution of 2-bromopyridine (1.94 g, 16.7 mmol), **3** (4.0 g, 16.7 mmol), 2 M aqueous solution of K₂CO₃ (5.93 g, 53.8 mmol) and Pd(PPh₃)₄ (0.47 g, 0.41 mmol) in THF (60 ml) was stirred under reflux 24 h at 70 °C. The resulting mixture was concentrated under reduced pressure, extracted with diethylether, and poured into water. The organic layer was washed with water three times and dried over anhydrous MgSO₄. The solvents were concentrated under reduced pressure, and the residue was purified by column chromatography with ethylacetate-*n*-hexane (1 : 3, v/v) to give a colorless liquid (2.6 g, 13.6 mmol, 81.4%).

¹H-NMR (400 MHz, CDCl₃): δ (ppm) = 8.74–8.71 (td, *J* = 1.4 and 4.7 Hz, 1H, ArH), 7.79–7.76 (m, 2H, ArH), 7.75–7.69 (m, 1H, ArH), 7.28 (sext, *J* = 4.5 Hz, 1H, ArH), 7.23–7.15 (m, 2H, ArH). IR: ν (cm⁻¹) = 1580, 1570, 1490, 1460, 1430, 1270, and 901.

2-(4-Dodecyl-2,3-difluorophenyl)pyridine (6). Quantities: **4** (4.0 g, 12.3 mmol), 2-bromopyridine (1.94 g, 12.3 mmol), Pd(PPh₃)₄ (0.47 g, 0.41 mmol), THF (60 ml), and 2 M aqueous solution of K₂CO₃ (5.93 g, 43.0 mmol).

The experimental procedure was as described previously and yielded a white solid (2.1 g, 5.27 mmol, 78.9%).

¹H-NMR (400 MHz, CDCl₃): δ (ppm) = 8.71 (d, *J* = 4.4 Hz, 1H, ArH), 7.77–7.74 (m, 2H, ArH), 7.64 (t, *J* = 7.8 Hz, 1H, ArH), 7.25 (m, 1H, ArH), 7.04 (t, *J* = 7.5 Hz, 1H, ArH), 2.69 (t, *J* = 7.7 Hz, 2H, Ar-CH₂-), 1.63 (quint, *J* = 7.7 Hz, 2H, Ar-CH₂-

CH₂-), 1.40–1.15 (m, 18H, -CH₂-), 0.87 (t, *J* = 7.0 Hz, 3H, -CH₃). IR: ν (cm⁻¹) = 2960, 2910, 2850, 1590, 1470, 843, and 719.

5-Butoxy-2-chloropyridine (8). A solution of 2-chloro-5-hydroxypyridine (**7**) (4.0 g, 30.8 mmol), 1-iodobutane (5.67 g, 30.8 mmol), and K₂CO₃ (0.48 g, 30.8 mmol) in 2-butanone (150 ml) was stirred under reflux for 24 h at 60 °C. The resulting suspension was concentrated under reduced pressure, extracted with diethylether, and the extract then washed with aqueous K₂CO₃ solution and finally water. The organic layer was dried over MgSO₄ and concentrated under reduced pressure. The residue was purified by column chromatography with chloroform to give a colorless liquid (5.18 g, 27.9 mmol, 91%).

¹H-NMR (400 MHz, CDCl₃): δ (ppm) = 7.44 (d, *J* = 3.2 Hz, 1H, ArH), 7.22–7.14 (m, 2H, ArH), 3.98 (t, *J* = 6.6 Hz, 2H, Ar-O-CH₂-), 1.77 (quint, *J* = 7.0 Hz, 2H, Ar-O-CH₂-CH₂-), 1.48 (sext, *J* = 7.4 Hz, 2H, -CH₂-CH₃), 9.69 (t, *J* = 7.5 Hz, 2H, -CH₃). IR: ν (cm⁻¹) = 2960, 2930, 2870, 1590, 1570, 1450, 1380, 1270, 1220, 1140, 1130, 1020, and 966.

2-(4-Dodecyl-2,3-difluorophenyl)-5-butoxypyridine (9). Quantities: **4** (3.0 g, 9.21 mmol), **8** (1.71 g, 9.21 mmol), Na₂CO₃ (3.27 g, 29.6 mmol) and Pd(PPh₃)₄ (0.26 g, 0.23 mmol), THF (40 ml).

The experimental procedure of Suzuki coupling was as described previously and yielded a white solid (2.10 g, 4.87 mmol, 53%).

¹H-NMR (400 MHz, CDCl₃): δ (ppm) = 8.38 (d, *J* = 3.1 Hz, 1H, ArH), 7.7 (dd, *J* = 2.0 and 8.8 Hz, 2H, ArH), 7.60 (t, *J* = 7.6 Hz, 1H, ArH), 7.29–7.24 (m, 1H, ArH), 7.0 (t, *J* = 7.0 Hz, 1H, ArH), 4.05 (t, *J* = 6.4 Hz, 2H, Ar-O-CH₂-), 2.67 (t, *J* = 7.5 Hz, 2H, Ar-O-CH₂-), 1.81 (quint, *J* = 7.0 Hz, 2H, Ar-O-CH₂-CH₂-), 1.62 (quint, *J* = 7.0 Hz, 2H, -CH₂-), 1.51 (sext, *J* = 7.4 Hz, 2H, -CH₂-CH₃), 9.89 (t, *J* = 7.5 Hz, 2H, -CH₃), 8.68 (t, *J* = 7.0 Hz, 2H, -CH₃). IR: ν (cm⁻¹) = 2910, 2850, 1590, 1580, 1480, 1450, 1300, 1270, 1030, and 895.

Synthesis of Pt complexes

Pt(F₂PPy)acac. A solution of K₂PtCl₄ (2.75 g, 6.63 mmol), **5** (2.60 g, 13.6 mmol) in 2-ethoxyethanol (40 ml) and water (13 ml) was heated to 80 °C for 18 h under nitrogen atmosphere. Afterwards, the reaction mixture was cooled to RT and concentrated under reduced pressure. The resulting red brown precipitate was extracted with chloroform and washed with water three times. The organic layer was dried over anhydrous MgSO₄, and concentrated under reduced pressure to give a yellow solid (4.4 g).

A solution of the resulting yellow solid (4.40 g), acetylacetone (1.31 g, 13.1 mmol), and Na₂CO₃ (5.54 g, 52.3 mmol) in 2-ethoxyethanol (100 ml) was stirred at 100 °C for 16 h under nitrogen atmosphere. The reaction mixture was diluted with water, and extracted with chloroform. The organic layer was washed with water, dried over anhydrous MgSO₄, and concentrated under reduced pressure. The residue was purified by column chromatography with chloroform-*n*-hexane (1 : 1, v/v) to give a yellow solid (1.94 g, 4.00 mmol, 60.4%).

$^1\text{H-NMR}$ (400 MHz, CDCl_3): δ (ppm) = 9.06 (td, $J = 0.8$ and 5.9 Hz, 1H, ArH), 8.02 (d, $J = 8.2$ Hz, 1H, ArH), 7.86 (t, $J = 7.9$ Hz, 1H, ArH), 7.33–7.28 (m, 1H, ArH), 7.17 (t, $J = 6.7$ Hz, 1H, ArH), 7.11–7.03 (m, 1H, ArH), 5.47 (s, 1H, $\text{CH}_3\text{-C}=\text{CH-C-CH}_3$), 2.00 (d, $J = 4.7$ Hz, 6H, $\text{CH}_3\text{-C}=\text{CH-C-CH}_3$). IR: ν (cm^{-1}) = 1580, 1530, 1490, 1260, 1110, 1020, 933, 908, and 876. Anal. Calcd for $\text{C}_{16}\text{H}_{13}\text{F}_2\text{NO}_2\text{Pt}$: C, 39.68; H, 2.71; N, 2.89. Found: C, 39.61; H, 2.52; N, 2.81%.

Pt(12F₂PPy)acac. Quantities: (i) K_2PtCl_4 (1.69 g, 4.07 mmol), **6** (3.0 g, 8.35 mmol), 2-ethoxyethanol (30 ml), and water (10 ml). (ii) Yellow solid (3.8 g), acetylacetone (0.81 g, 8.08 mmol), Na_2CO_3 (3.42 g, 32.3 mmol), and 2-ethoxyethanol (60 ml).

The experimental procedure for synthesis of the Pt complex was as described previously and yielded a yellow solid (1.64 g, 2.51 mmol, 61.7%).

$^1\text{H-NMR}$ (400 MHz, CDCl_3): δ (ppm) = 9.01 (d, $J = 6.0$ Hz, 1H, ArH), 7.96 (d, $J = 8.4$ Hz, 1H, ArH), 7.82 (t, $J = 7.6$ Hz, 1H, ArH), 7.15–7.09 (m, 2H, ArH), 5.47 (s, 1H, $\text{CH}_3\text{-C}=\text{CH-C-CH}_3$), 2.67 (t, $J = 7.9$ Hz, 2H, Ar- CH_2 -), 2.00 (d, $J = 4.0$ Hz, 6H, $\text{CH}_3\text{-C}=\text{CH-C-CH}_3$), 1.65 (quint, $J = 7.9$ Hz, 2H, Ar- $\text{CH}_2\text{-CH}_2$ -), 1.40–1.20 (m, 18H, $-\text{CH}_2$ -), 0.87 (t, $J = 7.2$ Hz, 3H, $-\text{CH}_2\text{-CH}_3$). IR: ν (cm^{-1}) = 2950, 2920, 2850, 1610, 1570, 1490, 1460, 1200, 1020, and 719. Anal. Calcd for $\text{C}_{28}\text{H}_{37}\text{F}_2\text{NO}_2\text{Pt}$: C, 51.53; H, 5.71; N, 2.15. Found: C, 51.61; H, 5.71; N, 2.11%.

Pt(12F₂PPyO4)acac. Quantities: (i) K_2PtCl_4 (1.45 g, 3.48 mmol), **9** (3.0 g, 6.95 mmol), 2-ethoxyethanol (30 ml), and water (10 ml). (ii) Yellow solid (3.5 g), acetylacetone (0.66 g, 6.63 mmol), Na_2CO_3 (2.81 g, 26.5 mmol), and 2-ethoxyethanol (60 ml).

The experimental procedure for synthesis of the Pt complex was as described previously and yielded a yellow solid (1.23 g, 1.70 mmol, 64%).

$^1\text{H-NMR}$ (400 MHz, CDCl_3): δ (ppm) = 8.72 (d, $J = 2.7$ Hz, 1H, ArH), 7.85 (d, $J = 10.4$ Hz, 1H, ArH), 7.40–7.36 (dd, $J = 2.8$ and 9.1 Hz, 1H, ArH), 7.07 (d, $J = 6.8$ Hz, 1H, ArH), 5.47 (s, 1H, $\text{CH}_3\text{-C}=\text{CH-C-CH}_3$), 4.06 (t, $J = 6.6$ Hz, 2H, Ar- O-CH_2 -), 2.67 (t, $J = 7.5$ Hz, 2H, Ar- CH_2 -), 2.00 (d, $J = 4.0$ Hz, 6H, $\text{CH}_3\text{-C}=\text{CH-C-CH}_3$), 1.81 (quint, $J = 7.0$ Hz, 2H, Ar- $\text{O-CH}_2\text{-CH}_2$ -), 1.64 (quint, $J = 7.5$ Hz, 2H, Ar- $\text{CH}_2\text{-CH}_2$ -), 1.57–1.46 (m, 2H, $-\text{CH}_2$ -), 1.4–1.2 (m, 18H, $-\text{CH}_2$ -), 0.99 (t, $J = 7.5$ Hz, 3H, $-\text{CH}_3$), 0.87 (t, $J = 6.8$ Hz, 3H, $-\text{CH}_3$). IR: ν (cm^{-1}) = 2920, 2850, 1570, 1520, 1490, 1460, 1390, 1260, 831, and 810. Anal. Calcd for $\text{C}_{32}\text{H}_{45}\text{F}_2\text{NO}_3\text{Pt}$: C, 53.03; H, 6.26; N, 1.93. Found: C, 53.24; H, 6.29; N, 1.87%.

Preparation of polarized emitting cells

$\text{Pt}(\text{F}_2\text{PPy})\text{acac}$, $\text{Pt}(12\text{F}_2\text{PPy})\text{acac}$, and $\text{Pt}(12\text{F}_2\text{PPyO4})\text{acac}$ were dissolved in six kinds of nematic LC compounds with different T_{NI} : 4-cyano-4'-*n*-pentyl-1,1'-biphenyl (5CB) (Tokyo Kasei) and five kinds of commercial nematic LCs for LCD. The commercial LCs were E7 (Merck), JD-7000XX (JNC), JD-5023XX (JNC), ZLI-4792 (Merck), and MLC-6608 (Merck), which were mixtures of various LC compounds. E7 consists of an eutectic mixture of 5CB, 4-cyano-4'-*n*-heptyl-1,1'-biphenyl, 4-cyano-4'-

n-octyloxy-1,1'-biphenyl, and 4-cyano-4''-*n*-pentyl-1,1',1''-terphenyl: their mass fractions are 51, 25, 16, and 8%, respectively. All the samples exhibit a nematic phase at ambient temperature: the T_{NI} of 5CB is 35 °C; E7: 59 °C; JD-5023XX: 76 °C; ZLI-4792: 95 °C; MLC-6608: 90 °C. $\text{Pt}(12\text{F}_2\text{PPy})\text{acac}$ (1.9 wt%) or $\text{Pt}(12\text{F}_2\text{PPy})\text{acac}$ (2.6 wt%) or $\text{Pt}(12\text{F}_2\text{PPy})\text{acac}$ (2.9 wt%)/LC mixtures were prepared. In the each case of Pt complex/5CB mixture, the concentrations of 1, 9 2.6, and 2.9 wt% are nearly equal to 1.0 mol%, respectively.

The LC mixture was injected into a glass cell. The glass cell was assembled with two glass plates: the gap between them was 5 μm , provided by a polyester film. On each glass substrate, a rubbed polyimide alignment layer was coated. The rubbing directions of the upper and bottom glass substrates were arranged in anti-parallel orientations.

Notes and references

- C. S. Peyratout, T. K. Aldridge, D. K. Crites and D. R. McMillin, *Inorg. Chem.*, 1995, **34**, 4484.
- T. Maruyama and T. Yamamoto, *J. Phys. Chem. B*, 1997, **101**, 3806.
- D. M. Roundhill, H. B. Gray and C. M. Che, *Acc. Chem. Res.*, 1989, **22**, 55.
- D. G. Nocera, *Acc. Chem. Res.*, 1995, **28**, 209.
- T. Fischer, R. Czerwieńiec, T. Hofbeck, M. M. Osminina and H. Yersin, *Chem. Phys. Lett.*, 2010, **486**, 53.
- M. A. Baldo, S. Lamansky, P. E. Burrows, M. E. Thompson and S. R. Forrest, *Appl. Phys. Lett.*, 1999, **75**, 4.
- M. A. Baldo, D. F. O'Brien, Y. You, A. Shoustikov, S. Sibley, M. E. Thompson and S. R. Forrest, *Nature*, 1998, **395**, 151.
- X. Y. Wang, A. D. Guerro and R. H. Schmehl, *J. Photochem. Photobiol., C*, 2004, **5**, 55.
- I. Ciofini, P. P. Laine, F. Bedioui and C. Adamo, *J. Am. Chem. Soc.*, 2004, **126**, 10763.
- W. Y. Wong and C. L. Ho, *Coord. Chem. Rev.*, 2009, **253**, 1709.
- J. Brooks, Y. Babayan, S. Lamansky, P. I. Djurovich, I. Tsyba, R. Bau and M. E. Thompson, *Inorg. Chem.*, 2002, **41**, 3055.
- B. W. Ma, P. I. Djurovich and M. E. Thompson, *Coord. Chem. Rev.*, 2005, **249**, 1501.
- S. W. Lai, H. W. Lam, W. Lu, K. K. Cheung and C. M. Che, *Organometallics*, 2002, **21**, 226.
- M. Jandke, P. Strohegl and J. Gmeiner, *Synth. Met.*, 2000, **111–112**, 177.
- M. P. Aldred, P. Vlachos, A. E. A. Contoret, S. R. Farrar, W. C. Tsoi, B. Mansoor, K. L. Woon, R. Hudson, S. M. Kelly and M. O'Neill, *J. Mater. Chem.*, 2005, **15**, 3208.
- Y. H. Yao, S. H. Yang and C. S. Hsu, *Polymer*, 2006, **47**, 8297.
- M. Millaruelo, L. S. Chinellato, Jr., J. L. Serrano, L. Oriol and M. Pinol, *J. Polym. Sci., Part A: Polym. Chem.*, 2007, **45**, 4804.
- J. Frischeisen, D. Yokoyama, A. Endo, C. Adachi and W. Brutting, *Org. Electron.*, 2011, **12**, 809.
- M. Grell and D. D. C. Bradley, *Adv. Mater.*, 1999, **11**, 895.
- M. O'Neil and S. M. Kelly, *Adv. Mater.*, 2003, **15**, 1135.
- T. Miteva, A. Meisel, M. Grell, H. G. Nothofer, D. Lupo, A. Yasuda, W. Knoll, L. Kloppenburg, U. H. F. Bunz, U. Scherf and D. Neher, *Synth. Met.*, 2000, **111–112**, 173.
- H. Mochizuki and T. Ikeda, *Thin Solid Films*, 2006, **499**, 147.
- M. Hasegawa, S. Kunisaki, H. Ohtsu and F. Werner, *Monatsh. Chem.*, 2009, **140**, 751.
- K. Driesen, C. Vaes, T. Cardinaels, K. Goossens, C. G. Walrand and K. Binnemans, *J. Phys. Chem. B*, 2009, **113**, 10575.
- Y. G. Galyametdinov, A. A. Knyazev, V. I. Dzhabarov, T. Cardinaels, K. Driesen, C. G. Walrand and K. Binnemans, *Adv. Mater.*, 2008, **20**, 252.
- H. Tsumatori, T. Harada, J. Yuasa, Y. Hasegawa and T. Kawai, *Appl. Phys. Express*, 2011, **4**, 011601.
- S. H. Liu, M. S. Lin, L. Y. Chen, Y. H. Hong, C. H. Tsai, C. C. Wua, A. Polock, Y. Chi, C. A. Chen, S. H. Chen and H. F. Hsu, *Org. Electron.*, 2011, **12**, 15.

-
- 28 Y. Wang, Y. Liu, J. Luo, H. Qi, X. Li, M. Nin, M. Liu, D. Shi, W. Zhu and Y. Cao, *Dalton Trans.*, 2011, **40**, 5046.
- 29 S. P. Jiang, K. J. Luo, Y. H. Wang, X. Wang, Y. Jiang and Y. Y. Wei, *Chin. Chem. Lett.*, 2011, **22**, 1005.
- 30 M. Ghedini, D. Pucci, A. Crispini and G. Barberio, *Organometallics*, 1999, **18**, 2116.
- 31 J. Brooks, Y. Babayan, S. Lamansky, P. I. Djurovich, I. Tsyba, R. Bau and M. E. Thompson, *Inorg. Chem.*, 2002, **41**, 3055.
- 32 D. A. K. Vezzu, J. C. Deaton, J. S. Jones, L. Bartolotti, C. F. Harris, A. P. Marchetti, M. Kondakova, R. D. Pike and S. Huo, *Inorg. Chem.*, 2010, **49**, 5107.
- 33 K. W. Wang, J. L. Chen, Y. M. Cheng, M. W. Chung, C. C. Hsieh, G. H. Lee, P. T. Chou, K. Chen and Y. Chi, *Inorg. Chem.*, 2010, **49**, 1372.
- 34 K. Kuwamura, T. Ikegami, S. Masuo, S. Machida, N. Tanaka and A. Itaya, *J. Photochem. Photobiol., A*, 2008, **200**, 232.